Superlattices and Microstructures 86 (2015) 292–299

Contents lists available at ScienceDirect

Superlattices and Microstructures

journal homepage: www.elsevier.com/locate/superlattices

The intersubband optical properties of a two-electron quantum dot-quantum well heterostructure

Rasit Aydin [a], Hatice Tas [b], Mehmet Sahin [b,*]

[a] Department of Physics, Faculty of Sciences, Selçuk University, 42075 Konya, Turkey
[b] Department of Material Science and Nanotechnology Engineering, Abdullah Gül University, Kayseri, Turkey

ARTICLE INFO

Article history:
Received 13 June 2015
Received in revised form 29 July 2015
Accepted 30 July 2015
Available online 30 July 2015

Keywords:
Multi-shell quantum dot
Negatively charged donor impurity
Optical transitions

ABSTRACT

In this paper, both linear and third-order nonlinear optical properties of two-electron in a semiconductor core/shell/well/shell quantum dot (QD) heterostructure for cases with and without a hydrogenic donor impurity have been investigated in a detailed manner as depending on the structure parameters. For this purpose, first, the energy eigenvalues and corresponding wave functions of the structure have been computed as a function of the layer thicknesses by means of the self-consistent solution of the Poisson and Schrodinger equations in envelope function effective mass approximation. Second, using these energy eigenvalues and their wave functions obtained from the calculations, both linear and third-order nonlinear optical properties of the multi-shell QD (MSQD) with two-electron have been determined as a function of the photon energies and shell thicknesses. Also, all procedures mentioned above have been repeated for negatively charged donor impurity (D^-) located in the center of the same structure. Finally, obtained results have been presented comparatively for cases with and without the impurity.

1. Introduction

In the last two decades, the zero dimensional QD hetero nanostructures have attracted the most attention among the semiconductor nanostructures because of their interesting physical properties and device applications based on principles of quantum mechanics. Hence, the electronic and optical properties of QDs have been intensively examined by many authors [1–4]. Recently, some optical properties of low-dimensional semiconductors QD, such as dipol transitions [5–7], oscillator strengths [8–10], linear [11–13] and nonlinear [14–16] optical absorption coefficients, photoionization cross-sections [17], and refractive indices [18–21], have been investigated both theoretically and experimentally.

On the other hand, the application of some external perturbations on QDs, for example, electrical and/or magnetic field, hydrostatic pressure, and temperature etc. induces some important changes on their electronic and optical properties. Therefore, these effects have been studied by many researchers [22–29]. Xie [30–32] has investigated the optical properties of double electron QD with different confinement potential shapes, Gaussian and Wood-Saxon potentials, depending on confinement strength, impurity and magnetic field in the effective mass approximation by using matrix diagonalization method and compact-density matrix approach. Sahin [33] has reported the optical properties of one- and two-electron spherical QD as a function of radius, light intensity and photon energy for cases with and without a hydrogenic donor impurity. Lu et al. [34] have examined the optical absorption coefficients and refractive indices of a double electron QD using compact-density

* Corresponding author.
E-mail addresses: raydin@selcuk.edu.tr (R. Aydin), hatice.tas@agu.edu.tr (H. Tas), mehmet.sahin@agu.edu.tr (M. Sahin).

http://dx.doi.org/10.1016/j.spmi.2015.07.066
0749-6036/

matrix approximation. Lu and Xie [35] have worked on an external electric field effects on optical properties of a QD with two-electron using perturbation method. In addition to these the same structure mentioned above has been investigated by Mengesha and Malnev [36], using both variation and perturbation methods to get its low energy levels and optical properties. All of these studies make serious contributions to intelligibility of the physical properties of these structures thoroughly.

In the literature, there is no reported study on the optical properties of the MSQD with double electron so far. In our previous study [37], we have reported a detailed investigation of the electronic properties of a MSQD with two-electron for cases with and without a donor impurity as a function of the core radius, shell thickness and well width. In this study, we have carried out the linear and third-order nonlinear optical properties of the same structure as a function of shell thickness and photon energy. The results have been analyzed depending on core radii and shell thicknesses, and probable reasons leading to these situations have been discussed in a detail. As a result of these analyses, in this contribution, we demonstrate that the optical properties of this structure are dependent strictly on its geometric parameters such as shell thicknesses.

2. Model and theory

In this study, we have considered a multi-shell spherical CdSe/ZnS/CdSe/ZnS quantum dot nanocrystal with two-electron. The CdSe core material with radius R_1 is coated with ZnS shell which has a wider band gap than that of the CdSe. The shell thickness is $T_s = R_2 - R_1$ and the well width is $T_w = R_3 - R_2$. The potential profile of the structure is shown in Fig. 1.

We have considered interacting two electrons in the structure. In the framework of effective mass approximation and BenDaniel–Duke boundary condition, the single particle Schrödinger equation with existing of the impurity is given as

$$\left[-\frac{\hbar^2}{2}\vec{\nabla}_r\left(\frac{1}{m_e^*(r)}\vec{\nabla}_r\right) - e\phi_{sc} - \frac{Ze^2}{\kappa(r)r} + V_e(r)\right]R_{n\ell}(r) = \varepsilon_{n\ell}R_{n\ell}(r). \tag{1}$$

Here, first term is kinetic energy term of the electron, $\hbar$ is reduced Planck constant, $m_e^*(r)$ is the position-dependent effective mass of the electron, e is the unit electronic charge, ϕ_{sc} is the self-consistent Hartree potential between the electrons, the third term is the Coulomb interaction between electron and donor impurity, Z is charge of the impurity, $V_e(r)$ is the position dependent confining potential of the electron, $\kappa(r)$ is the position dependent dielectric constant, $\varepsilon_{n\ell}$ is the single particle energy eigenvalue and $R_{n\ell}(r)$ is the radial wave function of the electron. It is noted that $Z = 1$ cases correspond to existing of the on-center impurity. In this case, the two-electron quantum structure is called as a negatively charged donor impurity (D^-). If $Z = 0$, the structure is called as a QD with two electrons.

The mathematical expression of the confining potential of the considered structure is given by

$$V_e(r) = \begin{cases} 0, & r \leqslant R_1 \quad \text{and} \quad R_2 \leqslant r \leqslant R_3 \\ V_b, & R_1 < r < R_2 \quad \text{and} \quad r > R_3 \end{cases}, \tag{2}$$

where V_b is the conduction band offset between CdSe and ZnS.

The electrostatic Coulomb potential originated from the interaction between electrons is calculated by solving of the Poisson equation. In the manner including interface polarization the Poisson equation can be expressed as

$$\vec{\nabla}\kappa(r)\vec{\nabla}\phi_{sc} = \frac{e}{\varepsilon_0}\rho_e(r), \tag{3}$$

where $\rho_e(r)$ is the electron density, and ε_0 is the dielectric permittivity of the vacuum. The electron density is determined by means of

$$\rho_e(r) = \frac{1}{4\pi}q\left|R^{elec}_{nq,\ell q}(r)\right|^2. \tag{4}$$

The details of the electronic structure calculation can be found elsewhere [37].

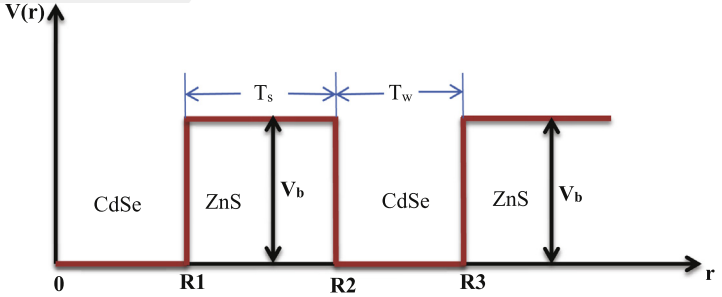

Fig. 1. The potential profile of multi-shell CdSe/ZnS quantum dot heterostructure.

The energy eigenvalues and corresponding wave functions obtained by self-consistent solution of Poisson–Schrödinger equations are used in order to determine the linear and third order nonlinear optical properties of the structure.

The oscillator strength is expressed as [39]

$$f_{ba} = \frac{2m}{\hbar^2}(E_a - E_b)|Z_{ba}|^2, \tag{5}$$

where Z_{ba} is the electric dipole matrix element and in a single electron system, square of the dipole matrix element for a $1s - 1p$ transition is

$$|Z_{ba}|^2 = \frac{1}{3}\left|\int_0^\infty R_{1,1}(r) r^3 R_{1,0}(r) dr\right|^2. \tag{6}$$

Here, $R_{1,0}(r)$ and $R_{1,1}(r)$ are radial wave functions of initial and final states, respectively.

In a quantum system with two-electron, the optical transition probability of an electron from an initial state to a final one by absorbing a photon is equivalent to each other and the dipole matrix element can be expressed as [34,35]

$$Z_{ba} = e < \psi_b|\mathbf{r}_1 + \mathbf{r}_2|\psi_a > . \tag{7}$$

The linear and third order nonlinear intersubband optical absorption coefficients are

$$\alpha^{(1)}(\omega) = \omega\sqrt{\frac{\mu}{\kappa}}\frac{N\hbar\Gamma_{ab}|Z_{ba}|^2}{(E_b - E_a - \hbar\omega)^2 + (\hbar\Gamma_{ab})^2}, \tag{8}$$

$$\alpha^{(3)}(\omega, I) = -\omega\sqrt{\frac{\mu}{\kappa}}\left(\frac{I}{2\varepsilon_0 n_r c}\right)\frac{4N\hbar\Gamma_{ab}|Z_{ba}|^4}{\left[(E_b - E_a - \hbar\omega)^2 + (\hbar\Gamma_{ab})^2\right]^2}, \tag{9}$$

respectively [33]. Here, c is speed of the light in the vacuum, w is the angular frequency of the light interacted with the MSQD, μ is the magnetic permeability of the material, I is the light intensity, $\hbar\Gamma_{ab}$ is the Lorentzian line width, κ and n_r are the dielectric constant and refractive index of the material, respectively, N is the electron density and is determined by $n/V_{KN}, n$ is the number of the electron and V_{KN} is the volume of the confined region.

The total absorption coefficient is calculated by means of

$$\alpha(\omega, I) = \alpha^{(1)}(\omega) + \alpha^{(3)}(\omega, I). \tag{10}$$

3. Results and discussion

The atomic units have been used throughout the calculations, where $\hbar = m_0 = e = 1$. The material parameters are $m^*_{CdSe} = 0.13m_0$ and $m^*_{ZnS} = 0.28m_0, \kappa_{CdSe} = 9.3$ and $\kappa_{ZnS} = 8.1, n_r = 2.6$, the electron confinement potential is $V_b = 1.05$ eV [38]. Here, the Lorentzian peak width is chosen as $\hbar\Gamma_{ab} = 3.28$ meV. The effective Bohr radius and the effective Rydberg energy are determined as $a_0 = 37.84$ Å and $R_y = 20.44$ meV, respectively.

The probability distribution and single particle energy levels of ground ($1s$) and excited ($1p$) states of two-electron MSQD for $Z = 0$ and $Z = 1$ cases at different core radii are shown in Fig. 2. As seen from the figure, both ground and excited state

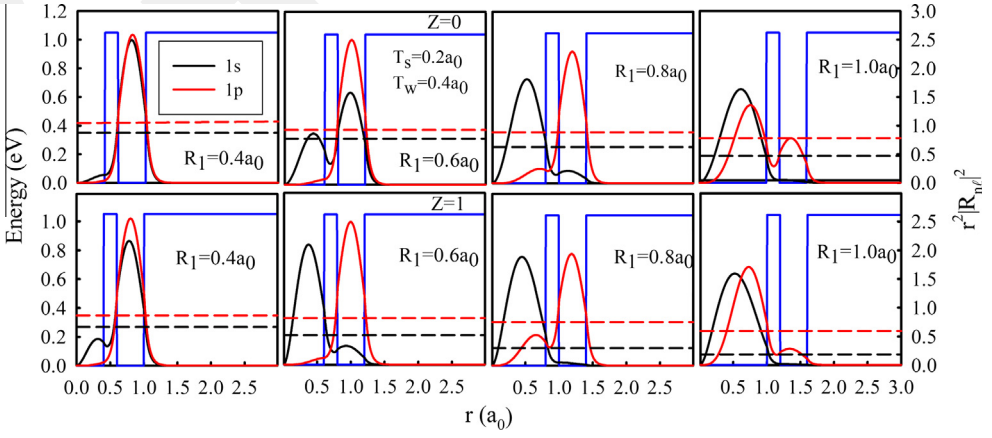

Fig. 2. The probability densities and single particle energy levels of ground ($1s$) and excited ($1p$) states depending on core radius R_1, for the cases $Z = 0$ (upper panel) and $Z = 1$ (bottom panel), where shell thickness is $T_s = 0.2a_0$ and well width is $T_w = 0.4a_0$.

energies exhibit a decreasing tendency with increasing R_1 since there is a relation between energy and size in the manner that $E \propto 1/R_1^2$. As shown in the bottom panel of the figure, in case of $Z = 1$, both ground and excited state energies are lower than that of $Z = 0$ cases (top panel). This is due to the attractive Coulomb potential of the impurity. The effect of the Coulomb potential is more dominant on the ground states when compared to excited ones and so the energy gap between $1s$ and $1p$ is larger for $Z = 1$ cases in comparison with $Z = 0$ cases. In Fig. 2, for $R_1 = 0.4a_0$ in case without impurity $Z = 0$, probability densities of both ground and excited states are localized in the well region. This situation results in the overlapping of wave functions becomes larger and the optical transition occurs in the well region. With the increasing of R_1, probability densities of both states start tunneling from the well region to the core one and with further increasing of R_1 the finding probabilities, especially for ground states, confine in the core region. On the other hand, as seen from the bottom panel of the same figure, in case with impurity ($Z = 1$) for $R_1 = 0.4a_0$, while excited state wave function localizes in the well region, ground state wave function localizes partly in the core region due to the impurity. So, in this case overlapping of the wave functions and dipole matrix element are slightly smaller than that without impurity. In the $Z = 1$ case, just as $Z = 0$, increasing of R_1 values leads to localize of probability densities in the core region.

In Fig. 3, the variations of linear, third order non-linear and total absorption coefficients with the incident light energy are given for different core radii both $Z = 0$ and $Z = 1$ cases. Here, black, red and green lines represent the linear, third order non-linear and the total absorption coefficients, respectively. Also, while dashed lines correspond to the case of $Z = 1$, the solid lines are for the case of $Z = 0$. As shown in the figure, in the resonance case, in which the photon energy is equal to the energy difference between excited and ground states, the absorption curve reaches its maximum value. From the figure, we can observe that the linear, third order non-linear and total absorption coefficients exhibit a decreasing tendency with increasing of the core radius until $R_1 = 1.0a_0$. When the radius become $R_1 = 1.0a_0$, the absorption coefficients begin to take larger values. This appearance is because of the inverse relation between the absorption coefficient and the volume of confining region as well as larger overlapping of the wave functions. As the linear absorption coefficient peak values are almost same for both $Z = 0$ and $Z = 1$ cases except for $R_1 = 0.6a_0$, the absolute value of the nonlinear absorption coefficients are much smaller for the case with the impurity. That is, the impurity plays a reducing effect on the nonlinear absorption coefficient for all core radii. We conclude that the overlapping of wave functions and so the absorption coefficient values become high for small core radii. On the other hand, with the increasing of core radius, probability densities of $1s$ and $1p$ levels are

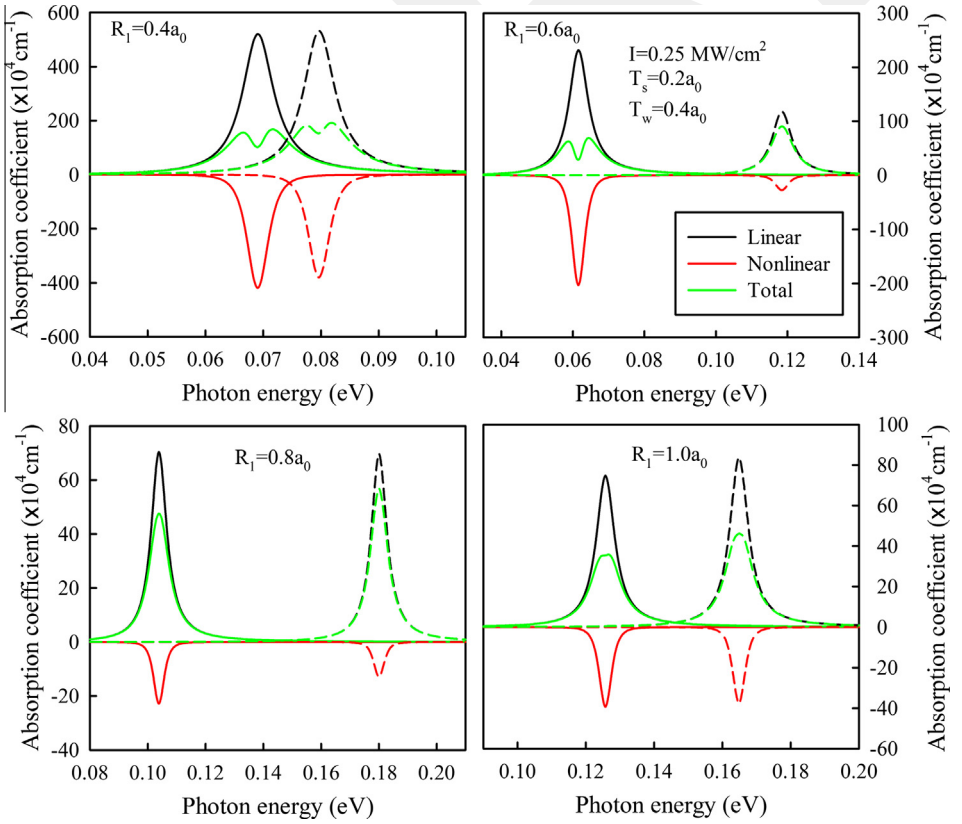

Fig. 3. The variation of linear, third-order nonlinear and total absorption coefficients with the incident photon energy, for the cases with $Z = 0$ (solid line) and $Z = 1$ (dashed line), where the barrier thickness is $T_s = 0.2a_0$, well width is $T_w = 0.4a_0$ and incident photon intensity is $I = 0.25$ MW/cm^2 for four core radii.

localized in different regions and hence dipole matrix element and absorption coefficient decrease. Further increase in the core radius results in an increase on overlapping of wave function and thus absorption coefficient increases again. When we look at Fig. 3, for $Z = 0$, the maximum values of absorption coefficients correspond to small photon energies whereas for $Z = 1$ this occurrence is seen in large photon energies. This stems from the increase between the energy difference $1s$ and $1p$ with the effect of impurity.

Fig. 4 shows the changes of the probability densities of $1s$ and $1p$ states for the cases with and without the impurity for different barrier thicknesses (T_s). As can be seen from the top panel of Fig. 4, in the case of $Z = 0$, although the density probability of ground and excited states tunnels a little to the core region, this tunneling decreases with increasing shell thickness and both of them are completely localized in the well region at larger shell thicknesses, and so the overlapping of the wave functions, and depending on this, the dipole matrix element goes to a large values. As a result of this, the optical transitions take place in this region. The bottom panel of Fig. 4 illustrates similar behaviors of cases without the impurity in general manner. However, since there exists an attractive Coulomb interaction of the impurity, the finding probability in the core region becomes larger at all shell thicknesses.

In Fig. 5, the variation of the linear, third order non-linear and total absorption coefficients with the incident photon energy is given for four different barrier thicknesses and $Z = 0$ and $Z = 1$. As seen from the figure, the peak value of absorption coefficient corresponds to larger photon energies for small shell thicknesses (T_s). At the same time, the linear absorption coefficient is larger at small shell thicknesses and becomes smaller with increasing shell thicknesses. In contrast to this, the nonlinear absorption coefficients increase as absolute values with increasing shell thicknesses. In addition, in small shell thicknesses, the impurity effect is more apparent on the energy levels and hence the peak energy values of absorption coefficients for cases with and without the impurity are separated from each other and this separation disappear at larger shell thicknesses because the shell thickness reduces the attractive effect of the impurity Coulomb potential. As a result, we conclude that the absorption strength, and its resonant transition energies can be easily controlled in MSQD heterostrucutres via adjusting of the shell thicknesses.

Fig. 6 shows the variation of probability densities of ground and excited states depending on well widths, T_w, for the cases with and without the impurity. According to the figure, we can infer that for the case $Z = 0$ and $T_w = 0.2a_0$ the probability density of ground state is localized in the well region considerably while this localization for excited state occurs totally in the well region. As a result of this, the overlapping of wave function and so dipole matrix element has large value. On the other hand, in case of $Z = 1$, while excited state wave function is still localized in well region, ground state wave function is much substantially localized in the core region due to the effect of attractive Coulomb potential of the impurity. Thus, both overlapping and dipole matrix element have small values as compared to the case of $Z = 0$. As the well widths increase, the probability densities of both ground and excited state are localized almost completely in the well region and their energies decrease significantly for $Z = 0$ and $Z = 1$ cases.

In Fig. 7, the dependency of linear, nonlinear and total absorption coefficients on the incident photon energy is shown for the cases $Z = 0$ and $Z = 1$ for four different well widths. Because the difference between initial and final energy states are larger for $Z = 1$ cases when it is compared with $Z = 0$ cases, the absorption spectra are separated from each other in small widths. With the increasing of the well width, T_w, the peak values of absorption coefficients shift to small photon energies (red shifting) and the absorption spectra overlap for the cases with and without the impurity. In small well widths, the absorption coefficients of $Z = 1$ case are smaller than that of $Z = 0$ because weaker overlapping as seen from Fig. 6. When the well width increases, the absorption coefficients of both $Z = 0$ and $Z = 1$ cases remain at almost same values. Besides, in large well widths, absorption coefficient values become smaller because of the larger confinement volumes. On the other hand, the linear absorption coefficients are affected more drastically with the well width when compared to nonlinear ones.

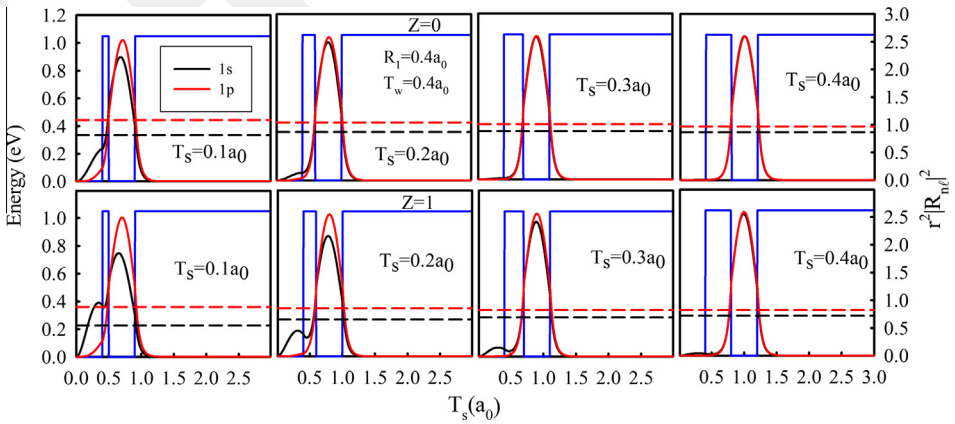

Fig. 4. The probability densities of ground ($1s$) and excited ($1p$) states depending on barrier thickness, for the cases of $Z = 0$ and $Z = 1$, where core radius is $R_1 = 0.4a_0$ and well width is $T_w = 0.4a_0$.

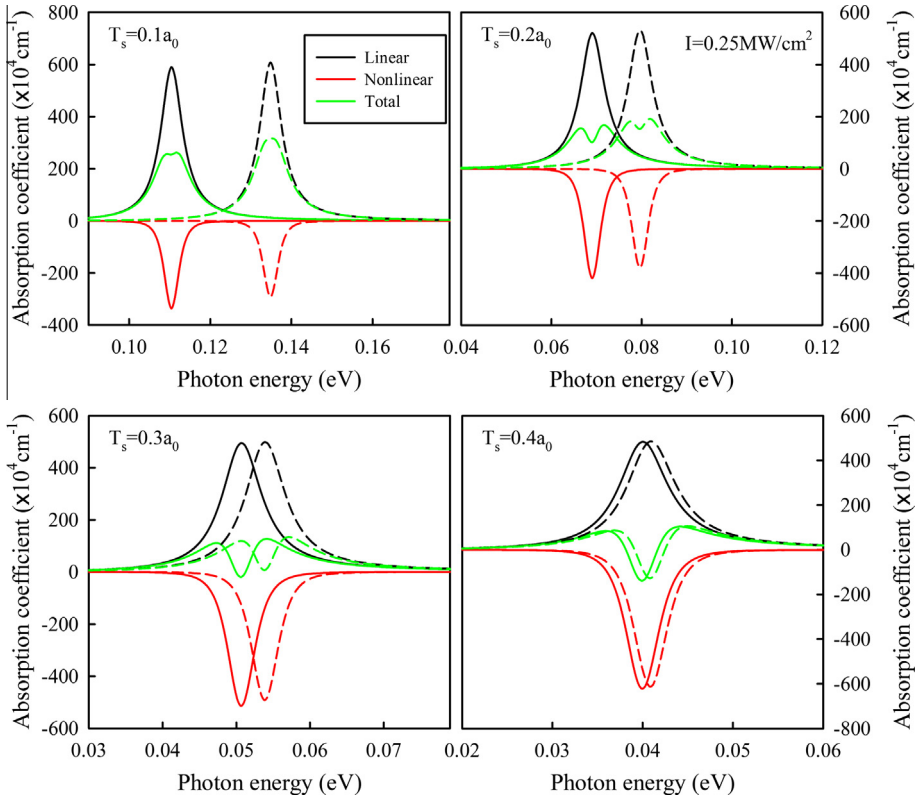

Fig. 5. The variation of linear, third-order nonlinear and total absorption coefficient with the incident photon energy, for the cases of $Z = 0$ (solid line) and $Z = 1$ (dashed line), where core radius is $R_1 = 0.4a_0$, well width is $T_w = 0.4a_0$ and incident photon intensity is $I = 0.25$ MW/cm^2, for four different barrier thicknesses.

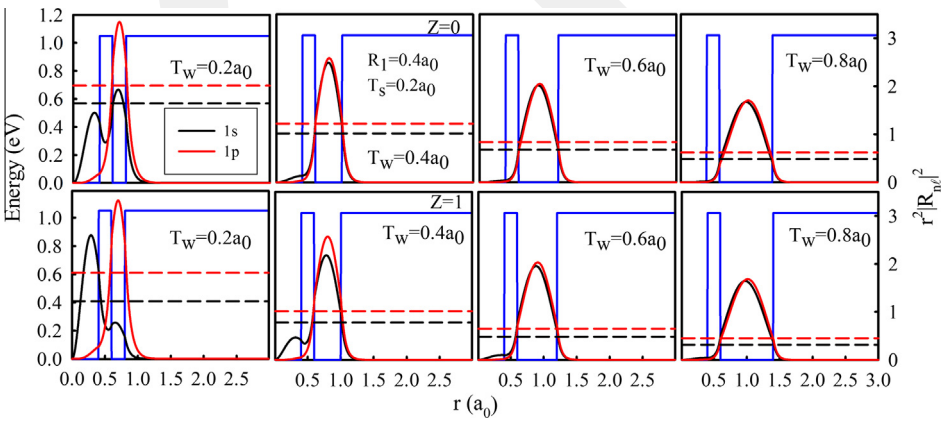

Fig. 6. The probability densities of ground and excited states depending on well width, for the cases $Z = 0$ and $Z = 1$, where shell thickness is $T_s = 0.2a_0$ and core radius is $R_1 = 0.4a_0$.

In Fig. 8, the variation of linear, non-linear and total absorption coefficients are plotted as a function of the incident light for three different light intensities. As can be seen from Eqs. (8) and (9), while linear absorption coefficient is not dependent on the light intensity, the non-linear absorption coefficient and thus total absorption one is directly proportional to the light intensity. This dependency is shown in Fig. 8 in the cases with and without impurity. Though the linear absorption coefficients in both $Z = 0$ and $Z = 1$ cases are approximately same, the non-linear absorption coefficients are a little smaller in $Z = 1$ than in $Z = 0$. Hence, the total absorption coefficient in $Z = 1$ case are larger than in $Z = 0$ case. There is a similar result to ours reported in some studies [39]. Also as can be seen from the figure, according to variation of the light intensity, although a bleaching does not seem in the total absorption coefficient for $I = 0.1$ MW/cm^2, it seems for $I = 0.2$ MW/cm^2

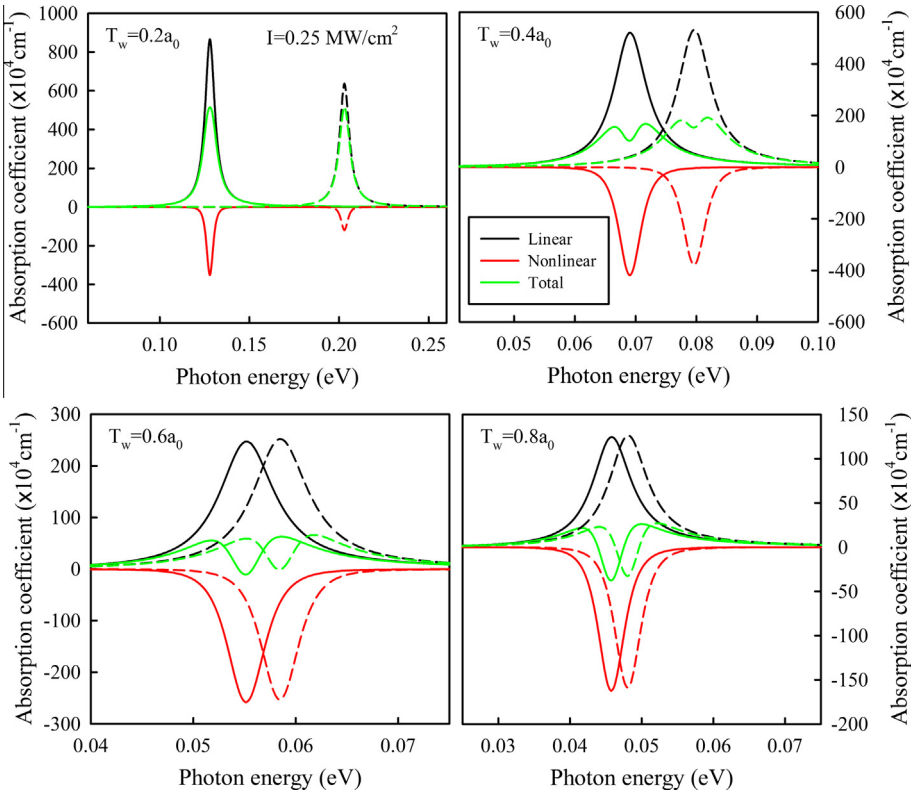

Fig. 7. The variation of linear, third order nonlinear and total absorption coefficient with the incident photon energy, for the cases $Z = 0$ (solid line) and $Z = 1$ (dashed line), where core radius is $R_1 = 0.4a_0$, barrier thickness is $T_s = 0.2a_0$ and incident photon intensity is $I = 0.25$ MW/cm^2, for four different well widths.

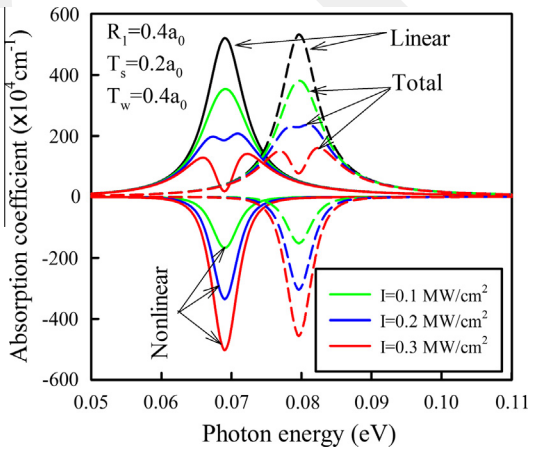

Fig. 8. The variation of linear, third-order nonlinear and total absorption coefficient with the incident photon energy, for the cases $Z = 0$ (solid line) and $Z = 1$ (dashed line), where core radius is $R_1 = 0.4a_0$, barrier thickness is $T_s = 0.2a_0$, well width is $T_w = 0.2a_0$ and for three incident photons intensities.

and 0.3 MW/cm^2. The bleaching in the case $Z = 0$ are more apparent than that of $Z = 1$ case because non-linear absorption coefficient are slightly larger in $Z = 0$ case.

4. Conclusion

In this study, the linear and third order nonlinear optical properties of a multi-shell spherical quantum dot heterostructure with two-electron have been examined comprehensively for the cases with and without a hydrogenic donor impurity.

The variation of absorption coefficients with the layer thicknesses of structure and light intensity have been investigated and discussed deeply for the cases $Z = 0$ and $Z = 1$. As a consequence of these calculations, we observe that the impurity has an important effect especially on the nonlinear absorption coefficients. We believe that this study will stimulate researchers to carry out experimental studies of nonlinear optical properties of MSQD with two-electron, and contribute to better understanding of these type of zero-dimensional quantum heterostructures.

Acknowledgments

This work is a part of the Ph.D. thesis preparing by R. Aydin at Physics Department of Selcuk University. One of the authors (M.S.) thanks Foundation of Abdullah Gul University (AGUV) for their financial support.

References

[1] J-L. Zhu, J-J. Xiong, B-L. Gu, Phys. Rev. B 41 (1990) 6001.
[2] E.C. Niculescu, A. Niculescu, Mod. Phys. Lett. 11 (1997) 673.
[3] N.V. Lien, N.M. Trinh, J. Phys. Condens. Matter 13 (2001) 2563.
[4] A.J. Peter, Physica E 28 (2005) 225.
[5] W. Xie, Physica B 403 (2008) 4319.
[6] R. Kostic, D. Stojanovic, Phys. Scr. T149 (2012) 014055.
[7] A. Keshavarz, N. Zamani, Superlattices Microstruct. 58 (2013) 191.
[8] V.G. Stoleru, E. Towe, Appl. Phys. Lett. 83 (2003) 5026.
[9] S. Yilmaz, H. Safak, Physica E 36 (2007) 40.
[10] B. Bochorishvili, H.M. Polatoglu, IOP Conf. Series: Mater. Sci. Eng. 6 (2009) 012026.
[11] A. Ozmen, Y. Yakar, B. Cakir, U. Atav, Opt. Commun. 282 (2009) 3999.
[12] B.D. Geyter, Z. Hens, Appl. Phys. Lett. 97 (2010) 161908.
[13] G. Rezaei, B. Vaseghi, N.A. Doostimotlagh, Commun. Theor. Phys. 57 (2012) 485.
[14] M.R.K. Vahdani, G. Rezaei, Phys. Lett. A 373 (2009) 3079.
[15] B. Cakir, Y. Yakar, A. Ozmen, M.O. Sezer, M. Sahin, Superlattices Microstruct. 47 (2010) 556.
[16] Y. Yakar, B. Cakir, A. Ozmen, Commun. Theor. Phys. (2010) 531185.
[17] M. Sahin, F. Tek, A. Erdinc, J. Appl. Phys. 111 (2012) 084317.
[18] W. Yao, Z. Yu, Y. Liu, B. Jia, Physica E 41 (2009) 1382.
[19] G. Rezaei, Z. Mousazadeh, B. Vaseghi, Physica E 42 (2010) 1477.
[20] G. Rezaei, M.R.K. Vahdani, B. Vaseghi, Physica B 406 (2011) 1488.
[21] Gh. Safarpour, M. Barati, J. Lumin. 137 (2013) 98.
[22] Z.H. Zhang, K.X. Guo, B. Chen, R.Z. Wang, M.W. Kang, S. Shao, Superlattices Microstruct. 47 (2010) 325.
[23] E. Sadeghi, Superlattices Microstruct. 50 (2011) 331.
[24] M. Kirak, S. Yilmaz, M. Sahin, M. Gencaslan, J. Appl. Phys. 109 (2011) 094309.
[25] W. Xie, Solid State Commun. 151 (2011) 545.
[26] Q. Wu, K. Guo, G. Liu, J.H. Wu, Physica B 410 (2013) 206.
[27] B.A. Farkoush, Gh. Safarpour, A. Zamani, Superlattices Microstruct. 59 (2013) 66.
[28] M. Kirak, Y. Altinok, S. Yilmaz, J. Lumin. 136 (2013) 415.
[29] G. Rezaei, S.S. Kish, Superlattices Microstruct. 53 (2013) 99.
[30] W. Xie, J. Phys: Condens. Matter 21 (2009) 115802.
[31] W. Xie, Opt. Commun. 284 (2011) 4756.
[32] W. Xie, Quantum Electron. 43 (2013) 71.
[33] M. Sahin, J. Appl. Phys. 106 (2009) 063710.
[34] L. Lu, W. Xie, H. Hassanabadi, J. Appl. Phys. 109 (2011) 063108.
[35] L. Lu, W. Xie, Phys. Scr. 84 (2011) 025703.
[36] M. Mengesha, V. Malnev, Superlattices Microstruct. 52 (2012) 1.
[37] R. Aydin, M. Sahin, J. Appl. Phys. 114 (2013) 043706.
[38] M. Sahin, S. Nizamoglu, A.E. Kavruk, H.V. Demir, J. Appl. Phys. 106 (2009) 043704.
[39] J.H. Davies, The Physics of Low-dimensional Semiconductors: An Introduction, Cambridge University Press, 1997.